AGU PUBLICATIONS

Geophysical Research Letters

RESEARCH LETTER
10.1002/2018GL077167

Key Points:
- We developed a framework to evaluate how surface fluxes and shallow mixing affect the isotopic composition of the MBL vapor
- The validity of the model is demonstrated against observations representative of various oceanic conditions
- It complements the existing mixing models, which were not adapted to take into account the isotopic fractionation during evaporation

Supporting Information:
- Supporting Information S1
- Text S1
- Data Set S2

Correspondence to:
M. Benetti,
marioncb@hi.is

Citation:
Benetti, M., Lacour, J.-L., Sveinbjörnsdóttir, A. E., Aloisi, G., Reverdin, G., Risi, C., et al. (2018). A framework to study mixing processes in the marine boundary layer using water vapor isotope measurements. *Geophysical Research Letters, 45*, 2524–2532. https://doi.org/10.1002/2018GL077167

Received 13 OCT 2017
Accepted 15 FEB 2018
Accepted article online 20 FEB 2018
Published online 10 MAR 2018

A Framework to Study Mixing Processes in the Marine Boundary Layer Using Water Vapor Isotope Measurements

M. Benetti[1], J.-L. Lacour[1], A. E. Sveinbjörnsdóttir[1], G. Aloisi[2], G. Reverdin[2], C. Risi[3], A. J. Peters[4], and H. C. Steen-Larsen[4,5]

[1]Institute of Earth Sciences, University of Iceland, Reykjavik, Iceland, [2]Sorbonne Université/CNRS/IRD/UPMC, LOCEAN, Paris, France, [3]Laboratoire de Météorologie Dynamique, IPSL, Sorbonne Universités UPMC, CNRS, Paris, France, [4]Bermuda Institute of Ocean Sciences, St. George's, Bermuda, [5]Geophysical Institute, Bjerknes Centre for Climate Research, University of Bergen, Bergen, Norway

Abstract We propose a framework using water vapor isotopes to study mixing processes in the marine boundary layer (MBL) during quiescent conditions, where we expect evaporation to contribute to the moisture budget. This framework complements the existing models, by taking into account the changing isotopic composition of the evaporation flux (δ_e), both directly in response to the mixing and indirectly in response to mixing and surface conditions through variations in MBL humidity. The robustness of the model is demonstrated using measurements from the North Atlantic Ocean. This shows the importance of considering the δ_e variability simultaneous to the mixing of the lower free troposphere to the MBL, to simulate the MBL water vapor, whereas a mixing model using a constant δ_e fails to reproduce the data. The sensitivity of isotope observations to evaporation and shallow mixing further demonstrates how these observations can constrain uncertainties associated with these key processes for climate feedback predictions.

1. Introduction

As a result of ongoing global warming, significant changes in moisture fluxes in the marine boundary layer (MBL) are expected (Bintanja & Selten, 2014; Durack et al., 2013). Yet our current knowledge of processes controlling humidity in the MBL, and in turn cloudiness, remains imprecise and has been identified to dominate the wide spread in estimated climate sensitivities (Bony & Dufresne, 2005; Webb et al., 2006). In particular, recent studies have stressed the need to better represent shallow mixing at the top of the MBL (Sherwood et al., 2014) and its interplay with surface heat fluxes in climate models (Brient et al., 2016; Vial et al., 2016). In this context, observations of water vapor isotopes ($\delta^{18}O$ and δD) and deuterium excess (d-excess = $\delta D - 8 \times \delta^{18}O$; Dansgaard, 1964), which are sensitive to both the mixing and the surface heat fluxes, have potential for constraining the representation of these processes (e.g., Bailey et al., 2013; Benetti et al., 2014; Kurita, 2013).

The isotope data are, however, not straightforward to interpret, and frameworks to interpret them are therefore needed. Isotope-enabled general circulation models (e.g., Galewsky et al., 2016; Risi et al., 2010) can be used to assist in interpreting isotope variations; however, specific processes can be difficult to identify owing to the complexity of general circulation models (e.g., Steen-Larsen et al., 2017). Another approach is to use a closure assumption to deduce δ_{MBL} assuming that all the water vapor in the MBL originates from local evaporation, neglecting inputs from the free troposphere (Merlivat & Jouzel, 1979, hereinafter MJ79). However, simulating δ_{MBL} without taking into account mixing processes leads to systematic biases (Jouzel & Koster, 1996). In a more realistic framework, the MBL water vapor can be considered as the result of mixing between the free troposphere and the evaporative flux. Mixing models between two air parcels can be elaborated from mass balance equations (Galewsky & Hurley, 2010; Noone et al., 2011) to deduce information on the moistening/dehydrating processes in the atmosphere (e.g., Conroy et al., 2016; Lacour et al., 2017; Worden et al., 2007). Usually, these mixing models use constant values for the two end-members and the moist and enriched end-member is often set as the water saturated at the ocean surface or as the subtropical water vapor. However, in the MBL, where we expect a strong evaporative contribution to the water vapor budget, simulating the mixing requires a constantly changing evaporative source (δ_e), since δ_e is a function of surface conditions (Craig & Gordon, 1965). Previously, Benetti et al. (2014) proposed a mixing model

between two vapor fluxes that integrates a changing δ_e simulated by the Craig and Gordon equation (CGE) (Craig & Gordon, 1965) with mixing of the lower free troposphere (LFT) water vapor. They showed that the δ_e variability and the LFT contribution (from LMDz-iso) were required to simulate temporal series of δ_{MBL} during a period of moderate trade winds with weak sea surface temperature (SST) variability.

Here we aim to offer a general framework to characterize mixing processes in the MBL during quiescent weather (distinct from periods of convective activity), and we seek the simplest conceptual 1-D framework to reproduce the specific humidity (q) and δ_{MBL} distribution. We take advantage of a data set with a large spatiotemporal coverage to discuss the model for different oceanic regions and seasons over the North Atlantic.

2. Methods

2.1. The MBL-Mix Model

This study generalizes the use of the model elaborated in Benetti et al. (2014) (see their appendix for the full description) in order to expand its application field. The model simulates δ_{MBL} as the result of instantaneous mixing of the evaporative source calculated by the CGE with an air mass from the LFT (see Figure 1a). The simplified mixing process is represented by (1), with r being the proportion of water vapor from the LFT incorporated into the MBL and with δ_e calculated by the CGE (2).

$$\delta_{MBL} = (1 - r).\delta_e + r.\delta_{LFT} \tag{1}$$

$$1 + \delta_e = \frac{1}{\alpha_k}.\frac{\alpha_{eq}^{vl}.(1 + \delta_{OC}) - RHS.(1 + \delta_{MBL})}{1 - RHS} \tag{2}$$

where RHS is the relative humidity normalized to SST, α_{eq}^{vl} the equilibrium fractionation factor between vapor and liquid, and α_k the kinetic fractionation factor. We use α_{eq}^{vl} from Majoube (1971) and α_k for smooth regime ($\alpha_k{}^{18}O = 1.006$ and $\alpha_k D = 1.0053$) (Merlivat & Jouzel, 1979).

As in MJ79 closure, we combine (1) and (2) and solve the resulting expression for δ_{MBL} (3) (to avoid specifying δ_{MBL} in the CGE). Equation (3) is then used iteratively by varying the proportion of water vapor from the LFT into the MBL (r).

$$\delta_{MBL} = (1 - b).\delta_{m79} + b.\delta_{LFT} \tag{3}$$

with $b = \frac{r.\alpha_k.(1-RHS)}{(1-r).RHS+\alpha_k.(1-RHS)}$ and δ_{m79}, the isotopic composition of the evaporated flux calculated from MJ79 closure (see equation in supporting information).

Simple mass balance calculations show that the proportion of water vapor from the LFT mixed into the MBL is equal to the specific humidity of the dry source over the MBL ($r = q_{LFT}/q_{MBL}$) (see calculations in Appendix A of Benetti et al., 2014). The key difference here compared to MJ79 closure is in the formulation of equation (1) because δ_{MBL} is calculated as a function of r rather than set equal to δ_e. This allows us to calculate RHS as a function of SST, r, and q_{LFT} (RHS = $q_{LFT}/r/q_s$(SST)). Compared to MJ79 closure, the interest of MBL-mix arises from (1) taking into account the mixing with the LFT and (2) calculating RHS interactively rather than prescribing it. As a consequence, three additional processes are taken into account: (1) direct effect of mixing on δ_{MBL}; (2) indirect effect of r on δ_{MBL} through its effect on q_{MBL}, thus on RHS, and thus on δ_e; and (3) indirect effect of SST on δ_{MBL} through its effect on RHS and thus on δ_e. In return, the model needs specified LFT properties.

The different relationships between δD, $\delta^{18}O$, q, and d-excess simulated by MBL-mix are presented in Figure 1. We also show a simple mixing model using a constant δ_e (no kinetic processes) and the result of the closure assumption (no mixing processes). With MBL-mix, the most enriched and humid point corresponds to the equilibrium vapor with the ocean where q is at saturation. As drier air is progressively added into the MBL as a result of mixing with the LFT, δ_{MBL} and q decrease and at $r = 1$, q and δ are equal to the drier source characteristics. As mixing with the drier source increases, δ_e (shown in color) decreases, owing to increasing kinetic processes caused by lower q. In the δD-q space (Figure 1b), the MBL-mix relationship is similar to the hyperbolic path simulated by the mixing curve using a constant δ_e, while MBL-mix in $\delta^{18}O$-q exhibits a distinctive path with a steeper curve closer to equilibrium than the simple mixing curve (Figure 1c). The distinct

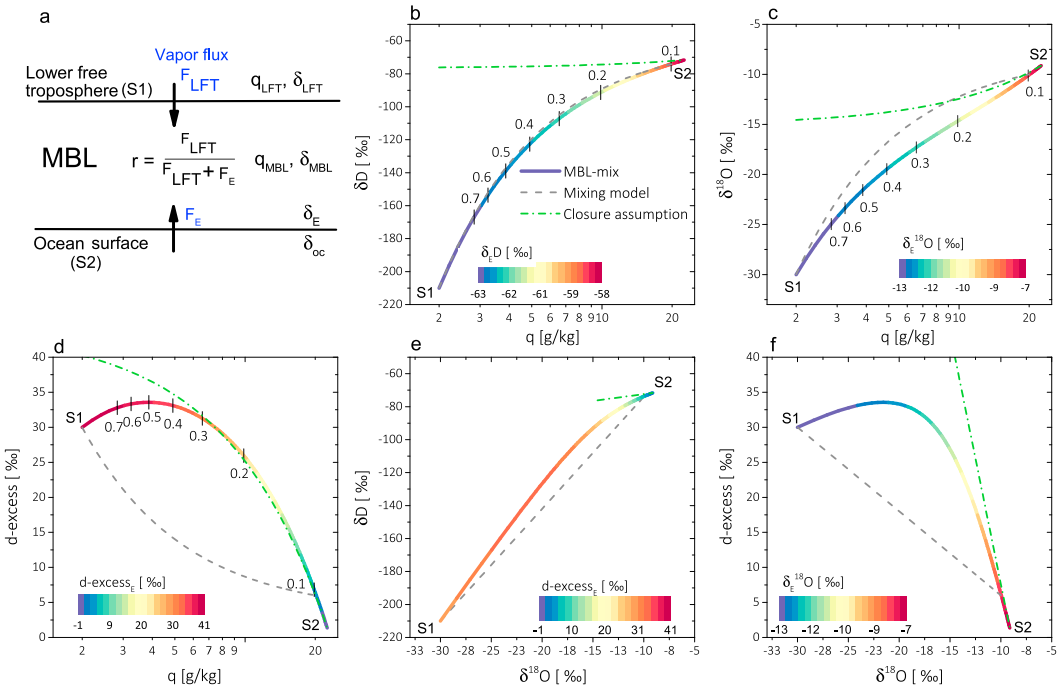

Figure 1. (a) Schematic cartoon of the MBL-mix model. Simulations of (b) δD-*q*, (c) δ^{18}O-*q*, (d) d-excess-*q*, (e) δD-δ^{18}O, and (f) d-excess-δ^{18}O by the MBL-mix model, a mixing model using a constant δ_e and the closure assumption. For MBL-mix model, the values of δ_e and d-excess$_e$ are indicated in colors and the proportion of the dry source (*r*) is shown along the curve. The humid and enriched end-member of the mixing model is a vapor close to the value measured in the subtropical ocean (q = 19 g/kg, δD = −78‰, δ^{18}O = −10‰, and d-excess = 2‰). The drier source is the same for the mixing model and MBL-mix (q = 2 g/kg, δD = −210‰, δ^{18}O = −30‰, and d-excess = 30‰). The surface conditions used in MBL-mix are SST = 27°C, δ_{OC}D = 0‰, and $\delta_{OC}{}^{18}$O = 0‰. The equations and Matlab functions used for Figure 1 are provided in the supporting information.

behaviors are a result of the different relative importance of the kinetic processes on $\delta^{18}O_{MBL}$ and δD_{MBL} ($\Delta\delta_e{}^{18}O \approx \Delta\delta_e D$, while $\Delta\delta D_{MBL} >> \Delta\delta^{18}O_{MBL}$). For the same reason, in the δD-δ^{18}O diagram (Figure 1e), MBL-mix simulates a lower slope (~4) for a high proportion of the evaporation flux compared to the mixing curve (~6.5). Such a low slope is impossible to reproduce with a simple mixing curve (constant δ_e), using a reasonable estimation of the triplet *q*-δD-δ^{18}O for the dry term, and clearly reflects the kinetic effects. Notice that MJ79 closure simulates an unrealistic low slope (~1), resulting only from kinetic processes. For the d-excess-*q* and d-excess-δ^{18}O relationships (Figures 1d and 1f), the model presents a high slope for large contribution of vapor from evaporation, as for the closure assumption. The model predicts a bell shape for the two relationships and indicates that high d-excess values can be reached during high proportion of mixing, owing to the strong kinetic effect responding to the dry surface conditions and even for a low d-excess in the LFT.

2.2. Data

We use MBL-mix during quiescent weather conditions, where we can consider that δ_{MBL} results from mixing between evaporation and air from the LFT. Typically, these conditions are prevalent during trade wind regimes, shallow cumulus, or clear sky. In deep convective situations, one can expect an influence of rain reevaporation, and knowing of the characteristics of convective downdrafts would be necessary to apply the model, which is beyond the goal of this paper.

2.2.1. MBL In Situ Measurements

We use the data sets published in Benetti, Reverdin, et al. (2017) and Benetti, Steen-Larsen, et al. (2017), covering a large part of the North Atlantic Ocean, and continuous MBL measurements carried out during the years 2011–2014 from a marine atmospheric observatory located on Bermuda (32.26°N, 64.88°W) (Steen-Larsen et al., 2014). From the data set in Benetti, Reverdin, et al. (2017) and Benetti, Steen-Larsen, et al. (2017) we retain two scientific cruises, STRASSE in 2012 and RARA AVIS in 2015, from 15°N to 50°N, in which we

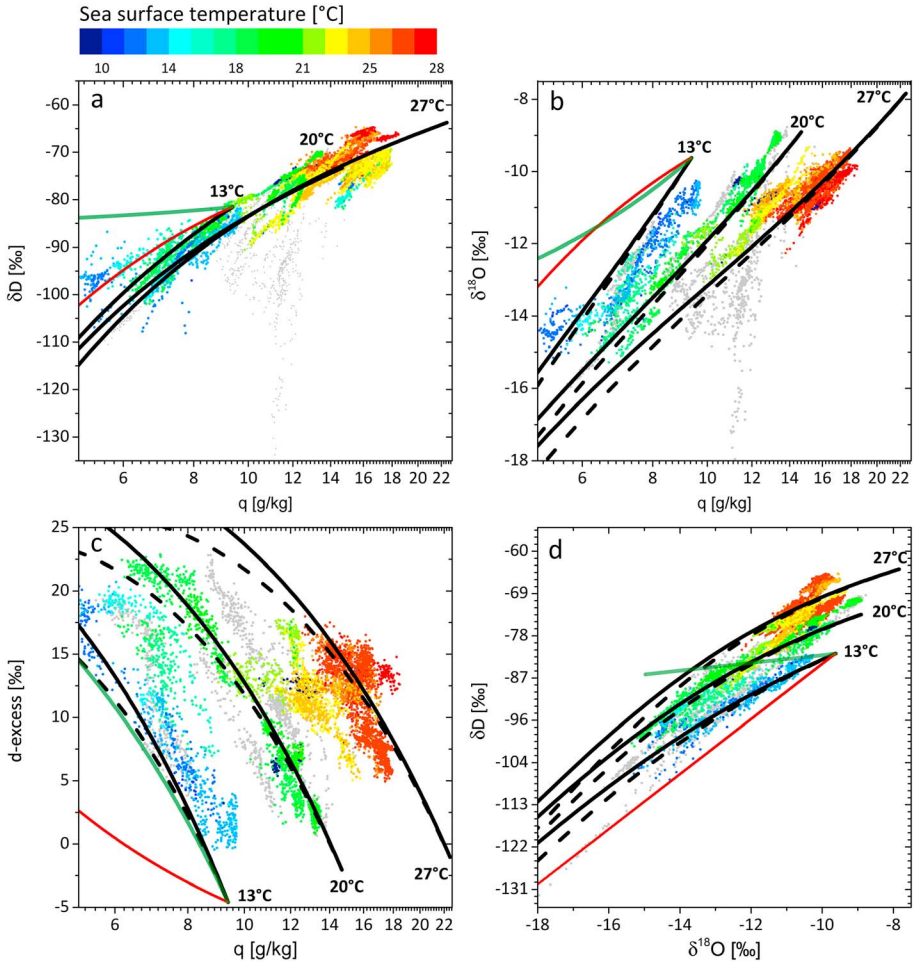

Figure 2. Relationships (a) δD-*q*, (b) δ^{18}O-*q*, (c) d-excess-*q*, and (d) δD-δ^{18}O in the water vapor over the Atlantic Ocean obtained from research vessels. The gray dots are data collected during convective events. The simulations from MBL-mix are shown for different ocean conditions: (13°C, $\delta^{18}O_{oc}$ = 0.7‰, and δD_{oc} = 4.5‰), (20°C, $\delta^{18}O_{oc}$ = 0.8‰, and δD_{oc} = 5.5‰), and (27°C, $\delta^{18}O_{oc}$ = 1.3‰, and δD_{oc} = 8.5‰) (average observations from the cruises; Benetti, Reverdin, et al., 2017; Benetti, Steen-Larsen, et al., 2017). MBL-mix simulations using different LFT d-excess are shown with black solid (30‰) and dashed (15‰) lines. A mixing curve with a constant δ_e (equal to the equilibrium water vapor at 13°C) is shown by the red line (the dry term is the same as used for the MBL-mix model with the high d-excess value). The closure model is shown by the green line for 13°C.

expect to have situations of mixing between the LFT and the MBL (trade winds in the subtropical region or clear sky/shallow cumulus observed in the midlatitudes). Nevertheless, four convective events were encountered during the cruises with precipitation and deep convective clouds. The corresponding data are presented with gray dots in Figure 2 and are not expected to be representative of the mixing conditions discussed in this paper. The data set and their calibrations are fully described in Benetti, Reverdin, et al. (2017), Benetti, Steen-Larsen, et al. (2017), and Steen-Larsen et al. (2014). We use 15 and 30 min averages for the cruise data and for the Bermuda data, respectively.

2.2.2. Characterization of the LFT

MBL-mix requires an estimate of the drier source end-members for *q*, δD, and δ^{18}O. We assume that the dry source characterizes the LFT. Whereas observations of δD in the LFT are derived from spaceborne instruments such as the Tropospheric Emission Spectrometer (TES) (Worden et al., 2012) or the Infrared Atmospheric Sounding Interferometer (Lacour et al., 2012), very few observations of δ^{18}O are available. Here we use δD profiles retrieved from TES to build a climatology of *q* and δD, selecting values at 3.5 km during 2009–2012 (see supporting information for further details). To consider a range of possible d-excess$_{LFT}$, we calculate $\delta^{18}O_{LFT}$ assuming d-excess$_{LFT}$ of 15 or 30‰.

For the cruise measurements, we use the medians of δD_{LFT} and q_{LFT} computed in the subtropics and at the midlatitudes, to account for spatial variations. Then, we calculate the $\delta^{18}O_{LFT}$ values that correspond to the two choices of d-excess$_{LFT}$ (15 and 30‰). The four LFT end-members are given in the supporting information. As expected with the latitudinal gradient, the LFT at midlatitudes (q = 1.70 g/kg) is drier and more depleted than the one calculated for the subtropical region (q = 2.14 g/kg).

When investigating the Bermuda measurements, we use the first and third quartiles of δD_{LFT} and q_{LFT} over a domain centered on Bermuda to estimate the possible variability with time. Then, we calculate the $\delta^{18}O_{LFT}$ value that corresponds to two choices of d-excess$_{LFT}$ (we apply the higher d-excess value to the first quartile, giving the drier end-member). The two LFT end-members are given in the supporting information. Here the q_{LFT} and δ_{LFT} difference between the two LFT (first and third quartiles) is large and reflects the diversity of LFT characteristics observed at Bermuda over several years.

3. Results and Discussions

In this section, we compare the model with the measurements from the North Atlantic cruises (section 3.1) and from the Bermuda marine station (section 3.2). The goals of this section are to assess the capacity of our model to capture the observed properties and to demonstrate its added value compared to MJ79 closure and to a simple mixing model between two constant end-members.

3.1. Spatial Variability

In Figure 2, we present the MBL-mix model simulations (black lines) for three different SST conditions spanning the subtropics in the summer to the midlatitudes in the winter: 27°C, 20°C, and 13°C. We use the LFT estimated from midlatitudes for the 20°C and 13°C conditions and LFT estimated from the subtropics for the 27°C condition. For comparison, a simple mixing model with a constant δ_e and the MJ79 closure are shown for 13°C. MBL-mix simulations agree best with observations, compared to a simple mixing model (fails for the $\delta^{18}O$-q, d-excess-q, and $\delta^{18}O$-δD relationships) or MJ79 closure (fails for the δD-q, $\delta^{18}O$-q, and $\delta^{18}O$-δD relationships) (see Table S3 for the root-mean-square deviation calculations). This reflects the importance of considering the δ_e variability simultaneous to the mixing of the LFT to the MBL, to simulate the MBL water vapor. The root-mean-square deviation calculations suggest that the δD-q relationship can be reproduced only if considering the mixing processes, while the d-excess-q relationship can be reproduced only if considering the kinetic processes. However, the $\delta^{18}O$-δD and $\delta^{18}O$-q relationships are only reproduced by MBL-mix which considers both processes.

Our model shows the importance of SST in capturing the different distributions of observed δD-$\delta^{18}O$-q-XS relationships. SST acts through two different processes: (1) the saturated q changes with SST, following the Clausius-Clapeyron relationship, thus acting on RHS and (2) δ_e follows the equilibrium fractionation factor that decreases by 1.18‰ ($\delta_e{}^{18}O$) and 14‰ ($\delta_e D$) when SST increases from 13°C to 27°C. The gray dots correspond to convection events, which are not simulated by MBL-mix model. The δ-q slopes for these events are steeper than those predicted by a Rayleigh distillation (not shown) and suggest an input of water vapor from rain reevaporation (e.g., Field et al., 2010; Worden et al., 2007).

3.2. Seasonal Variability

Now we compare the MBL-mix model with the Bermuda data collected over 4 years to capture the seasonal variability of the mixing processes in the MBL. Summer (orange) and winter (blue) probability density functions (Botev et al., 2010) are shown in Figure 3 (autumn and spring present intermediary distributions and are not shown here). The data are compared to the MBL-mix model simulations using representative summer and winter SST for this region (27°C and 21°C, respectively). For each season we use the two different LFT defined earlier from TES measurements as bracketing the conditions. The data are also compared with a simple mixing model using a constant δ_e.

Winter and summer data show contrasting distributions with less variability of humidity and δ_{MBL} in summer compared to winter (consistent with buildup of the stable Bermuda-Azores high-pressure system). While the mixing curves using a constant δ_e fail to envelop the data, the MBL-mix simulations using the two different LFT envelop the winter data. The kinetic effects are particularly striking in winter as the data draw a distinctive curved pattern in the $\delta^{18}O$-q diagram compared to the δD-q diagram. That the MBL-mix simulations

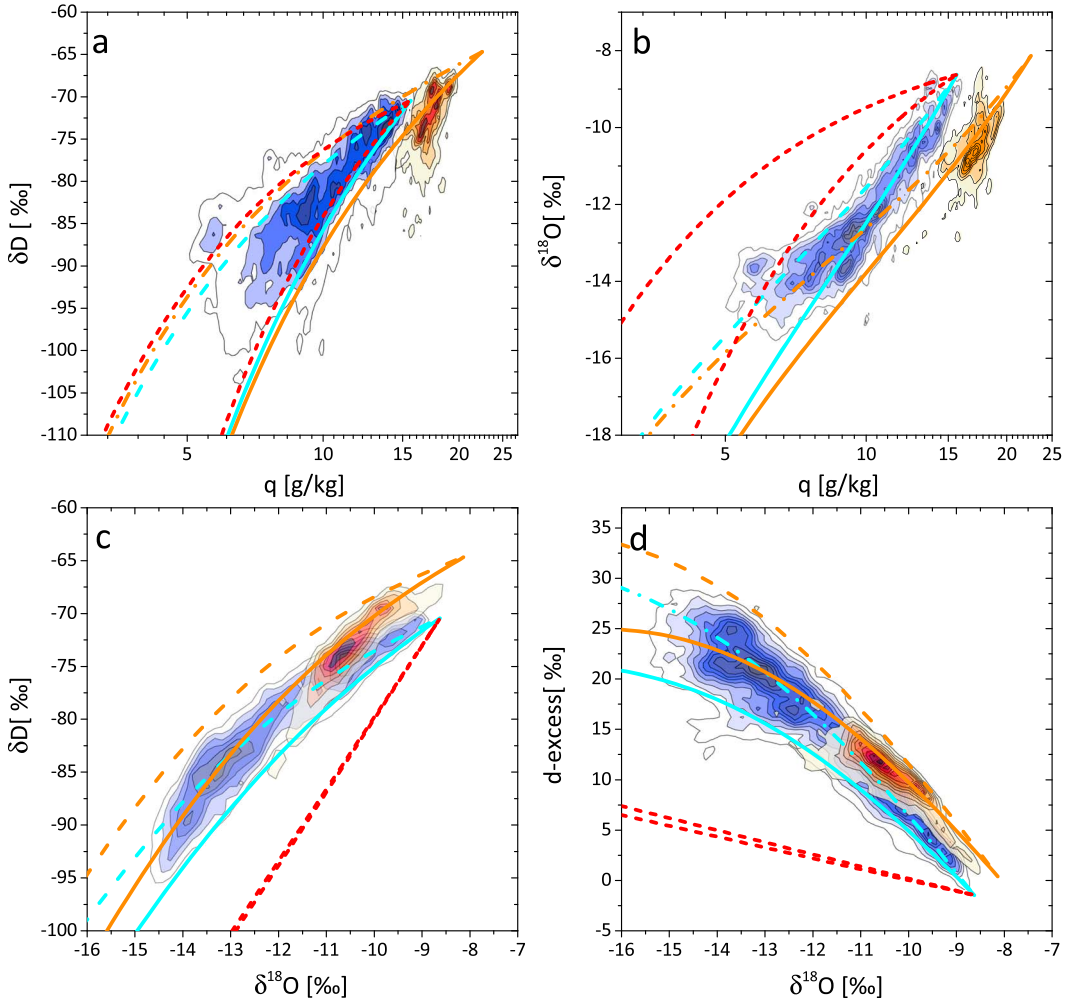

Figure 3. Relationships between (a) δD-*q*, (b) δ^{18}O-*q*, (c) δD-δ^{18}O, and (d) d-excess-*q* at Bermuda between 2011 and 2014. The summer data are shown in orange and the winter data in blue. MBL-mix simulations are calculated for summer shown in orange (SST = 27°C) and for winter shown in cyan (SST = 21°C). Two different LFT are shown for each SST (full line for LFT with a d-excess of 15‰ and dashed line for LFT with a d-excess of 30‰). Simple mixing curves are shown in red for winter conditions, using the same LFT end-members as in MBL-mix, and the humid end-member corresponds to the equilibrium water vapor at 21°C.

encompass the winter data suggests that the δ_{MBL} in winter at Bermuda is mainly controlled by the mixing between a variety of dry sources reasonably bounded by the LFT conditions described in section 3.2. The correspondence in the four diagrams of the data with an evaporative source simulated with the local SST (21°C) suggests a local contribution of evaporation during winter.

3.3. Discussion

In the previous section, our framework has been benchmarked against data, revealing the relevance of such a model to simulate isotopes in the MBL. Despite the simplified physical processes assumed by the model, this framework illustrates how the MBL properties respond to the drying due to the mixing with LFT and to the subsequent δ_e variability. We show that the spatial variability of SST is important to consider in order to represent the different relationships at the North Atlantic scale. To apply the model, the main difficulty is to estimate the properties of the LFT. Nevertheless, our study reveals that MBL-mix can work despite these uncertainties. The cruise data reveal that when the proportions of LFT air are relatively weak compared to evaporation, the model is not overly sensitive to the LFT properties (see full and dashed lines in Figure 2). On the other hand, the long-term model-data comparison at Bermuda shows the necessity to consider

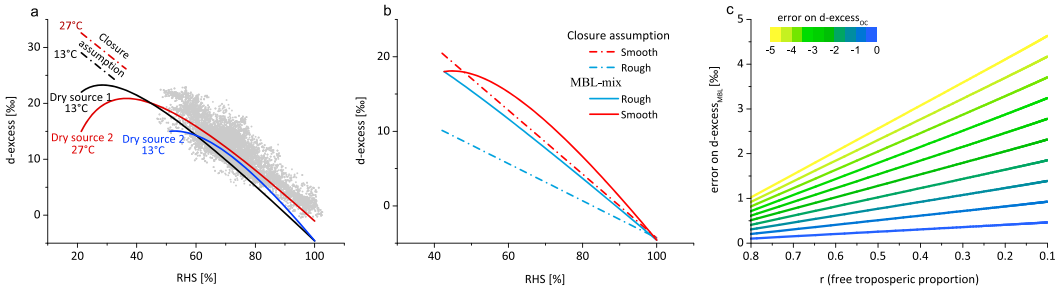

Figure 4. (a) The d-excess-RHS relationship. Simulations from MBL-mix are reported with 13°C and 27°C (similar dry sources as Figure 2) (full lines). Simulations from the closure assumption are reported with 13°C and 27°C (dashed lines). (b) The d-excess-RHS relationship from the closure assumption and MBL-mix model for the smooth and rough regimes. The dry source used for the MBL-mix model is q_{LFT} = 4 g/kg and d-excess$_{LFT}$ = 18‰. (c) Simulation of the error on d-excess$_{MBL}$ resulting from different approximations on d-excess$_{oc}$ (color scale) as a function of the proportion of free tropospheric vapor. The error is computed as the difference between the d-excess$_{MBL}$ computed from the approximated d-excess$_{oc}$ with the d-excess$_{MBL}$ computed from the true d-excess$_{oc}$.

both δ_{LFT} and q_{LFT} variability to encompass the observations during wintertime, suggesting the potential of inverting MBL isotope observations to derive information on LFT (e.g., Galewsky & Rabanus, 2016).

4. Examples of Applications

4.1. The Dependency of the RHS-d-excess Relationship to SST

The MJ79 closure predicts a dependence of the RHS-d-excess relationship to SST with increasing d-excess values for increasing SST (see Figure 4a). Since then, a number of observational studies have challenged the link between d-excess in the MBL and SST (e.g., Steen-Larsen et al., 2015, 2017). In the cruise data set, the relationship between d-excess and SST is apparently absent, despite the large SST range (see supporting information). Figure 4a presents the RHS-d-excess relationship predicted by MBL-mix for simulations using two different SST values (13°C and 27°C) with different LFT end-members. This example suggests that the mixing of the evaporative flux with different dry terms can erase the dependency predicted by MJ79 closure except for high RHS situations. The simulated d-excess-RHS relationships have similar slopes to the one predicted by MJ79 closure which suggests that this is a robust information that can be retrieved from d-excess$_{MBL}$ (Benetti et al., 2014; Uemura et al., 2008).

4.2. The Dependency of the RHS-d-excess Relationship to the Wind Regime

Now we use the model to evaluate how the free tropospheric mixing can affect the MBL water vapor response to evaporation during rough and smooth regime (Merlivat & Jouzel, 1979). Figure 4b shows the d-excess-RHS relationships for the smooth regime ($u_{10m} < 7$ m.s, $\alpha_k{}^{18}$O = 1.006, and α_kD = 1.0053) and rough regime ($u_{10m} > 7$ m.s, $\alpha_k{}^{18}$O = 1.0035, and α_kD = 1.0031) simulated by MJ79 closure (dashed line) and by MBL-mix (continuous line). The MBL-mix model shows how the effect of the two wind regimes on the kinetic fractionation can be altered by the mixing. This alteration is less or stronger as a function of the LFT characteristics.

4.3. Importance of Accurately Representing the Isotopic Composition at the Ocean Surface

The model can be used to evaluate the impact of approximations made on d-excess$_{OC}$ for simulated d-excess$_{MBL}$. The error on d-excess$_{MBL}$ resulting from the error on d-excess$_{OC}$ is expressed as a function of the proportion of LFT in the MBL (r) (Figure 4c). An error of 2‰ on d-excess$_{OC}$ can lead to an error of 2‰ for d-excess$_{MBL}$ when r = 0.2 (see supporting information for δ^{18}O and δD calculations). We suggest that to better simulate δ_{MBL} and d-excess$_{MBL}$ in regions of strong evaporation, one should integrate the mapped distributions of LeGrande and Schmidt (2006) (e.g., Werner et al., 2011) or use coupled ocean-atmosphere models (e.g., Werner et al., 2016).

5. Conclusions and Perspectives

We have developed a framework to study mixing processes in the MBL, where we expect evaporation to contribute to the moisture budget. This framework complements the existing models, by taking into account the

changing δ_e, both directly in response to the mixing and indirectly in response to mixing and surface conditions through variations in q_{MBL} humidity. The distinctive pathway portrayed by MBL-mix better reproduces δ_{MBL} than a mixing model using a constant δ_e or than the MJ79 closure assumption. Although the model framework assumes a 1-D stationary situation, the validity of our model is demonstrated against observations representative of various oceanic conditions and therefore we believe that it can be adopted by the water isotope and MBL community.

Our framework allows for a comprehensive and quantitative analysis on how surface fluxes and shallow mixing affect the isotopic composition of the MBL vapor. It reveals the necessity of considering both evaporation and mixing processes to simulate δ_{MBL} for a larger range of conditions than in Benetti et al. (2014). Given the sensitivity of MBL isotope to shallow mixing and surface heat fluxes, we suggest that isotope measurements could be used to constrain the representation of these processes in climate models which is of prime importance for better defining the uncertainty associated with the climate sensitivity (Sherwood et al., 2014; Vial et al., 2016).

We acknowledge the limitations that only a single dry source is specified. For cases with large relative contribution of evaporation, uncertainties on the dry source characteristics play a minor role. The model has not been applied in the presence of deep convective events, although MBL-mix could then be adapted with a specific free tropospheric term, integrating the downdraft properties. Nevertheless, in that case, we expect also a stronger influence of rain reevaporation effect, which is more complex to model.

Acknowledgments
The Tudor Hill Marine Atmospheric Observatory in Bermuda is supported by the NSF OCE-1130395, and the assistance of Matthew Hayden is gratefully acknowledged. Observations at Bermuda were supported by the Danish Council for Independent Research—Natural Sciences grant 10-092850, the Carlsberg Foundation, the Icelandic Centre for Research—Equipment Fund grant 1202340031, and the Icelandic Research Fund grant 152229-052. STRASSE was supported by two LEFE/IMAGO grants (Strasse and Strasse/SPURS), with support from IPSL and OSU Ecce Terra. The authors acknowledge "Les Amis du Jeudi et du Dimanche" and Herve Legoff for the installation on the RARA AVIS. The authors thank the National Power Company of Iceland Landsvirkjun for their contribution to this research. The data at Bermuda are available in the supporting information. The cruise data are provided at http://cds-espri.ipsl.fr/isowvdataatlantic/.

References

Bailey, A., Toohey, D., & Noone, D. (2013). Characterizing moisture exchange between the Hawaiian convective boundary layer and free troposphere using stable isotopes in water. *Journal of Geophysical Research: Atmospheres*, *118*, 8208–8221. https://doi.org/10.1002/jgrd.50639

Benetti, M., Reverdin, G., Pierre, C., Merlivat, L., Risi, C., Steen-Larsen, H. C., & Vimeux, F. (2014). Deuterium excess in marine water vapor: Dependency on relative humidity and surface wind speed during evaporation. *Journal of Geophysical Research: Atmospheres*, *119*, 584–593. https://doi.org/10.1002/2013JD020535

Benetti, M., Reverdin, G., Aloisi, G., & Sveinbjörnsdóttir, Á. (2017). Stable isotopes in surface waters of the Atlantic Ocean: Indicators of ocean-atmosphere water fluxes and oceanic mixing processes. *Journal of Geophysical Research: Oceans*, *122*, 4723–4742. https://doi.org/10.1002/2017JC012712

Benetti, M., Steen-Larsen, H. C., Reverdin, G., Sveinbjörnsdóttir, Á. E., Aloisi, G., Berkelhammer, M. B., et al. (2017). Stable isotopes in the atmospheric marine boundary layer water vapour over the Atlantic Ocean, 2012–2015. *Scientific Data*, *4*, 160128. https://doi.org/10.1038/sdata.2016.128

Bintanja, R., & Selten, F. M. (2014). Future increases in Arctic precipitation linked to local evaporation and sea-ice retreat. *Nature*, *509*(7501), 479–482. https://doi.org/10.1038/nature13259

Bony, S., & Dufresne, J.-L. (2005). Marine boundary layer clouds at the heart of tropical cloud feedback uncertainties in climate models. *Geophysical Research Letters*, *32*, L20806. https://doi.org/10.1029/2005GL023851

Botev, Z. I., Grotowski, J. F., & Kroese, D. P. (2010). Kernel density estimation via diffusion. *The Annals of Statistics*, *38*(5), 2916–2957. https://doi.org/10.1214/10-AOS799

Brient, F., Schneider, T., Tan, Z., & Bony, S. (2016). Shallowness of tropical low clouds as a predictor of climate models' response to warming. *Climate Dynamics*, *47*, 433–449.

Conroy, J. L., Noone, D., Cobb, K. M., Moerman, J. W., & Konecky, B. L. (2016). Paired stable isotopologues in precipitation and vapor: A case study of the amount effect within western tropical Pacific storms. *Journal of Geophysical Research: Atmospheres*, *121*, 3290–3303. https://doi.org/10.1002/2015JD023844

Craig, H., & Gordon, L. I. (1965). Deuterium and oxygen 18 variations in the ocean and the marine atmosphere. Retrieved from http://yncenter.sites.yale.edu/sites/default/files/shen_jing_jan_2013.pdf

Dansgaard, W. (1964). Stable isotopes in precipitation. *Tellus*, *16*(4), 436–468. https://doi.org/10.1111/j.2153-3490.1964.tb00181.x

Durack, P. J., Wijffels, S. E., & Boyer, T. P. (2013). Chapter 28: Long-term salinity changes and implications for the global water cycle. *International Geophysics*, *103*, 727–757.

Field, R. D., Jones, D. B. A., & Brown, D. P. (2010). Effects of postcondensation exchange on the isotopic composition of water in the atmosphere. *Journal of Geophysical Research*, *115*, D24305. https://doi.org/10.1029/2010JD014334

Galewsky, J., & Hurley, J. V. (2010). An advection-condensation model for subtropical water vapor isotopic ratios. *Journal of Geophysical Research*, *115*, D16116. https://doi.org/10.1029/2009JD013651

Galewsky, J., & Rabanus, D. (2016). A stochastic model for diagnosing subtropical humidity dynamics with stable isotopologues of water vapor. *Journal of the Atmospheric Sciences*, *73*(4), 1741–1753. https://doi.org/10.1175/JAS-D-15-0160.1

Galewsky, J., Steen-Larsen, H. C., Field, R. D., Worden, J., Risi, C., & Schneider, M. (2016). Stable isotopes in atmospheric water vapor and applications to the hydrologic cycle. *Reviews of Geophysics*, *54*, 809–865. https://doi.org/10.1002/2015RG000512

Jouzel, J., & Koster, R. D. (1996). A reconsideration of the initial conditions used for stable water isotope models. *Journal of Geophysical Research*, *101*, 22,933–22,938. https://doi.org/10.1029/96JD02362

Kurita, N. (2013). Water isotopic variability in response to mesoscale convective system over the tropical ocean. *Journal of Geophysical Research: Atmospheres*, *118*, 10,376–10,390. https://doi.org/10.1002/jgrd.50754

Lacour, J.-L., Flamant, C., Risi, C., Clerbaux, C., & Coheur, P.-F. (2017). Importance of the Saharan heat low in controlling the North Atlantic free tropospheric humidity budget deduced from IASI δD observations. *Atmospheric Chemistry and Physics*, *17*(15), 9645–9663. https://doi.org/10.5194/acp-17-9645-2017

Lacour, J.-L., Risi, C., Clarisse, L., Bony, S., Hurtmans, D., Clerbaux, C., & Coheur, P.-F. (2012). Mid-tropospheric δD observations from IASI/MetOp at high spatial and temporal resolution. *Atmospheric Chemistry and Physics*, *12*(22), 10,817–10,832. https://doi.org/10.5194/acp-12-10817-2012

LeGrande, A. N., & Schmidt, G. A. (2006). Global gridded data set of the oxygen isotopic composition in seawater. *Geophysical Research Letters*, *33*, L12604. https://doi.org/10.1029/2006GL026011

Majoube, M. (1971). Fractionnement en oxygène 18 et en deutérium entre l'eau et sa vapeur. *Journal de Chimie Physique*, *68*, 1423–1436. https://doi.org/10.1051/jcp/1971681423

Merlivat, L., & Jouzel, J. (1979). Global climatic interpretation of the deuterium-oxygen 18 relationship for precipitation. *Journal of Geophysical Research*, *84*, 5029–5033. https://doi.org/10.1029/JC084iC08p05029

Noone, D., Galewsky, J., Sharp, Z. D., Worden, J., Barnes, J., Baer, D., et al. (2011). Properties of air mass mixing and humidity in the subtropics from measurements of the D/H isotope ratio of water vapor at the Mauna Loa Observatory. *Journal of Geophysical Research*, *116*, D22113. https://doi.org/10.1029/2011JD015773

Risi, C., Bony, S., Vimeux, F., & Jouzel, J. (2010). Water-stable isotopes in the LMDZ4 general circulation model: Model evaluation for present-day and past climates and applications to climatic interpretations of tropical isotopic records. *Journal of Geophysical Research*, *115*, D12118. https://doi.org/10.1029/2009JD013255

Sherwood, S. C., Bony, S., & Dufresne, J.-L. (2014). Spread in model climate sensitivity traced to atmospheric convective mixing. *Nature*, *505*(7481), 37–42. https://doi.org/10.1038/nature12829

Steen-Larsen, H. C., Risi, C., Werner, M., Yoshimura, K., & Masson-Delmotte, V. (2017). Evaluating the skills of isotope-enabled general circulation models against in situ atmospheric water vapor isotope observations. *Journal of Geophysical Research: Atmospheres*, *122*, 246–263. https://doi.org/10.1002/2016JD025443

Steen-Larsen, H. C., Sveinbjörnsdottir, A. E., Jonsson, T., Ritter, F., Bonne, J.-L., Masson-Delmotte, V., et al. (2015). Moisture sources and synoptic to seasonal variability of North Atlantic water vapor isotopic composition. *Journal of Geophysical Research: Atmospheres*, *120*, 5757–5774. https://doi.org/10.1002/2015JD023234

Steen-Larsen, H. C., Sveinbjörnsdottir, A. E., Peters, A. J., Masson-Delmotte, V., Guishard, M. P., Hsiao, G., et al. (2014). Climatic controls on water vapor deuterium excess in the marine boundary layer of the North Atlantic based on 500 days of in situ, continuous measurements. *Atmospheric Chemistry and Physics*, *14*(15), 7741–7756. https://doi.org/10.5194/acp-14-7741-2014

Uemura, R., Matsui, Y., Yoshimura, K., Motoyama, H., & Yoshida, N. (2008). Evidence of deuterium excess in water vapor as an indicator of ocean surface conditions. *Journal of Geophysical Research*, *113*, D19114. https://doi.org/10.1029/2008JD010209

Vial, J., Bony, S., Dufresne, J.-L., & Roehrig, R. (2016). Coupling between lower-tropospheric convective mixing and low-level clouds: Physical mechanisms and dependence on convection scheme. *Journal of Advances in Modeling Earth Systems*, *8*(4), 1892–1911. https://doi.org/10.1002/2016MS000740

Webb, M. J., Senior, C. A., Sexton, D. M. H., Ingram, W. J., Williams, K. D., Ringer, M. A., et al. (2006). On the contribution of local feedback mechanisms to the range of climate sensitivity in two GCM ensembles. *Climate Dynamics*, *27*(1), 17–38. https://doi.org/10.1007/s00382-006-0111-2

Werner, M., Haese, B., Xu, X., Zhang, X., Butzin, M., & Lohmann, G. (2016). Glacial–interglacial changes in $H_2{}^{18}O$, HDO and deuterium excess—Results from the fully coupled ECHAM5/MPI-OM Earth system model. *Geoscientific Model Development*, *9*(2), 647–670. https://doi.org/10.5194/gmd-9-647-2016

Werner, M., Langebroek, P. M., Carlsen, T., Herold, M., & Lohmann, G. (2011). Stable water isotopes in the ECHAM5 general circulation model: Toward high-resolution isotope modeling on a global scale. *Journal of Geophysical Research*, *116*, D15109. https://doi.org/10.1029/2011JD015681

Worden, J., Kulawik, S., Frankenberg, C., Payne, V., Bowman, K., Cady-Peirara, K., et al. (2012). Profiles of CH_4, HDO, H_2O, and N_2O with improved lower tropospheric vertical resolution from Aura TES radiances. *Atmospheric Measurement Techniques*, *5*(2), 397–411. https://doi.org/10.5194/amt-5-397-2012

Worden, J., Noone, D., Bowman, K., Beer, R., Eldering, A., Fisher, B., et al. (2007). Importance of rain evaporation and continental convection in the tropical water cycle. *Nature*, *445*(7127), 528–532. https://doi.org/10.1038/nature05508